Digital dispersion compensation for ultrabroad-bandwidth single-camera spectral-domain polarization-sensitive OCT

Amy L. Oldenburg[1,2,3] and Raghav K. Chhetri[1]

[1]*Department of Physics and Astronomy,*
[2]*Biomedical Research Imaging Center,*
University of North Carolina at Chapel Hill, Chapel Hill, NC 27599-3255

1. Introduction

Polarization-sensitive OCT is used to examine tissue microstructure by providing imaging of birefringent properties.[1] Single-camera spectral-domain polarization-sensitive OCT has been of recent interest, whereby a custom spectrometer is employed to simultaneously measure orthogonal polarization states scattered from the sample.[2,3,4] This avoids synchronization and triggering issues associated with multiple-camera setups. It also has the advantage that the optic axis can be extracted without polarization modulating the incident light. However, the disadvantage is that the line camera pixel-to-wavenumber nonlinearity requires either careful spectrometer alignment,[2] or digital compensation.[5]

In fact, this problem is further exacerbated in high resolution PSOCT systems as they require compensation over larger bandwidths. Here we report the construction of an ultrabroad-bandwidth PSOCT system using a single camera spectrometer similar to Baumann *et al* [2]. In order to enjoy the benefits of this instrument, we outline a method for digital dispersion compensation that removes the necessity for special camera alignment. We find that there are three non-negligible types of dispersion to consider: 1) the aforementioned camera pixel-to-wavenumber nonlinearity, 2) the refractive index dispersion in the sample itself, and 3) the dispersion imbalance between the arms of the OCT interferometer. The latter two were previously recognized for time-domain high-resolution OCT, where a digital dispersion compensation method was successfully employed to treat them both.[6] For our SDOCT application, we find that dispersion types 1 and 2 have the same functional effect and can be combined into one compensation step, and as such, much of the previous compensation method can be used. However, we find that it is necessary to add two steps to the analysis technique whereby the relative scaling and positioning of the two polarization images is adjusted to align the scatterers. We also find that better results are achieved by fitting to larger polynomial orders. We show how our technique provides high-resolution PSOCT with precise alignment between the orthogonal polarization images.

2. Methods

The single-camera SD-PS-OCT system is briefly described as follows (see Fig. 1). A Ti:Sapphire laser (Griffin, KMLabs, Inc.) provides 130nm of bandwidth centered near 800nm. A free-space interferometer contains quarter waveplates at 22.5° and 45° in the reference and sample arms, respectively. A polarizing beamsplitter at the interferometer output divides horizontally- (|H>) and vertically- (|V>) polarized light components. The spectrometer consists of a 20kHz 4096 pixel line scan CCD (Dalsa Pirahna), 200mm focal length lens, 600/mm grating, and collimated |H> and |V> beams incident on the grating at angles ±2.9° from Littrow, respectively. Each polarization state is thus imaged onto each half of the 4096 pixel camera, providing a maximum optical delay of 2.08mm. In this study, A-lines were acquired at 5kHz.

Optical Coherence Tomography and Coherence Domain Optical Methods in Biomedicine XV, edited by James G. Fujimoto, Joseph A. Izatt, Valery V. Tuchin, Proc. of SPIE Vol. 7889, 78891V · © 2011 SPIE · CCC code: 1605-7422/11/$18
doi: 10.1117/12.874198

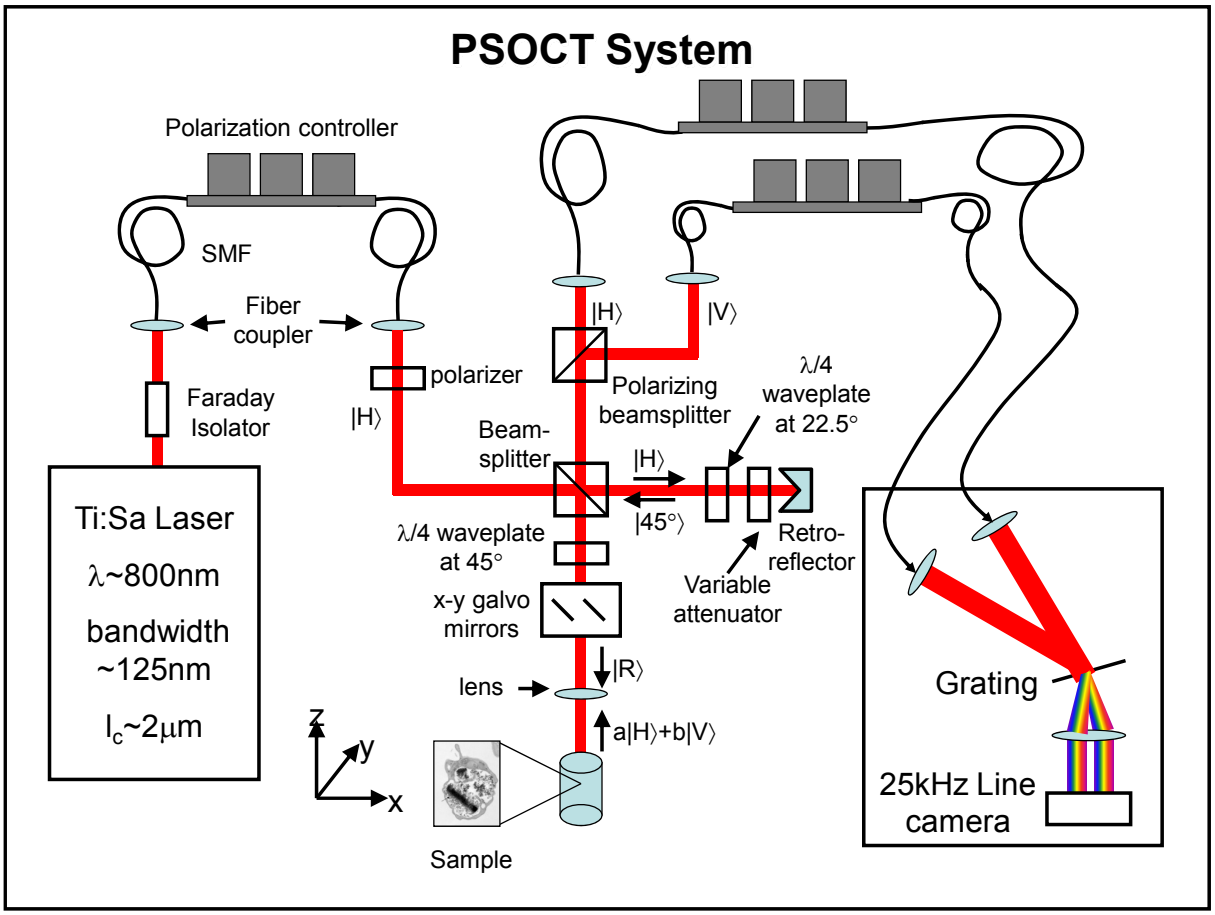

Fig. 1. PSOCT system diagram.

In an ideal system, the complex analytic signal corresponding to the spectral cross-correlation is:

$$\tilde{I}_D(k_s) \propto S(k_s) \sum_n \sqrt{R_{Sn}} \exp\left(i2k_s\left(z_R - z_{Sn}\right)\right)$$

where k_s is the wavenumber in the sample, and otherwise we have used the convention in [7]. Transform-limited image formation in the sample space z_s is achieved by Fourier transformation as follows:

$$\begin{aligned} F\left\{I_D(k_s)\right\} &\propto \gamma(z_s) \otimes \sum_n \sqrt{R_{Sn}}\,\delta\left(z_s - 2\left(z_R - z_n\right)\right) \\ &\propto \sum_n \sqrt{R_{Sn}}\,\gamma\left(2\left(z_R - z_n\right)\right) \end{aligned},$$

after ignoring the negative terms. To achieve transform-limited imaging computationally, it is necessary to convert the measured spectrum into an evenly sampled function in k_s. We note that a previously reported compensation method provides even sampling in free-space k by the use of a reference flat in the light beam,[5] but it does not correct for dispersion in the sample.

Realizing that frequency ω is invariant in all systems, we can write the measured spectral cross-correlation, which is evenly sampled in the camera pixel number p, as follows:

$$\tilde{I}_D\left(p(\omega)\right) \propto S\left(p(\omega)\right)\exp\left(i2\Delta k_{\text{int}}(\omega)z_R\right)\sum_n \sqrt{R_{Sn}}\exp\left(i2k_s(\omega)\left(z_R - z_{Sn}\right)\right)$$

where Δk_{int} is the dispersion mismatch in the interferometer. This first exponential term can be eliminated by multiplying the spectrum by a phase factor equal to $\phi = -2i\Delta k_{int} z_R$. The transformation from p to ω (camera nonlinearity) and ω to k_s (sample dispersion) can be compensated together by determining the relationship between p and k_s, then resampling the spectrum to achieve even sampling in k_s. To determine the appropriate phase and resampling factors, we analyze the top and bottom surface reflections of a water droplet. The steps taken are as follows:

Step 1: Apply a half-cosine to zero the |H> and |V> spectrum edges (20 pixels) for apodization. Pre-compensate by resampling to achieve reflection peaks that are sufficiently compact for further analysis. In this study we applied a 3rd order resampling polynomial using cubic spline.

Step 2: Compute the |H> and |V> spectroscopic phase difference between top and bottom surfaces (depth-dependent dispersion) by windowing the peaks in the time domain. Apply the pre-compensation to p to account for the effects of Step 1, fit $p(k_s)$ to a 7th order polynomial, and resample the spectrum. Find the new peak positions and compute the scaling difference (stretch) between the |H> and |V> images; modify the first-order term in the polynomial $p(k_s)$ for |V> to rescale it to match |H>.

Step 3: Compute the |H> and |V> spectroscopic phase of the top reflection peak only (fixed dispersion). Fit this phase ϕ to a 15th order polynomial and multiply the spectra by the inverse of this phase. Finally, locate the new top reflector peak positions and modify the first order term in ϕ of |V> to provide the correct time-domain shift to align the peaks.

The polynomial terms for ϕ and $p(k_s)$ are then stored for compensation of subsequent images.

3. Results and Discussion

First we demonstrate how OCT of a water droplet is analyzed to determine the dispersion parameters for aqueous samples. Figure 2 displays example time-domain A-line data at each step in the algorithm where the top air-water and bottom water-glass surfaces are indicated. (Note that the reflected light power is higher in |V> because of the waveplate settings). Before compensation the reflector peaks are too broad to be segmented for separate analysis (Fig. 2a), and the initial compensation step 1 is used to tighten these peaks (Fig. 2b). Then the depth-dependent dispersion parameters are computed in step 2 to give each reflector a constant dispersion and to adjust the relative length scaling (Fig. 2c). Finally, the fixed interferometer dispersion and sample position are compensated in step 3 (Fig. 2d), resulting in nearly transform-limited reflections that are aligned between polarization states. The full-width at half maximum in |H> was 6.7μm and 9.9μm (top and bottom) compared to the 3.7μm transform limit, and |V> was 4.2 μm and 5.8μm compared to the 4.4μm transform limit, in water. |V> exhibited better results than |H> because of its higher SNR when examining specular reflections; in future work |H> may be improved by using a referencing system that provides more cross-polarized scattering. We also found that the 3dB bandwidths for |H> and |V> were reduced to 58nm and 48nm because of chromatic effects from the waveplates. However, the 10dB bandwidth exceeded 140nm, dispersion parameter fitting over this large bandwidth was consistent, and future work will address this issue.

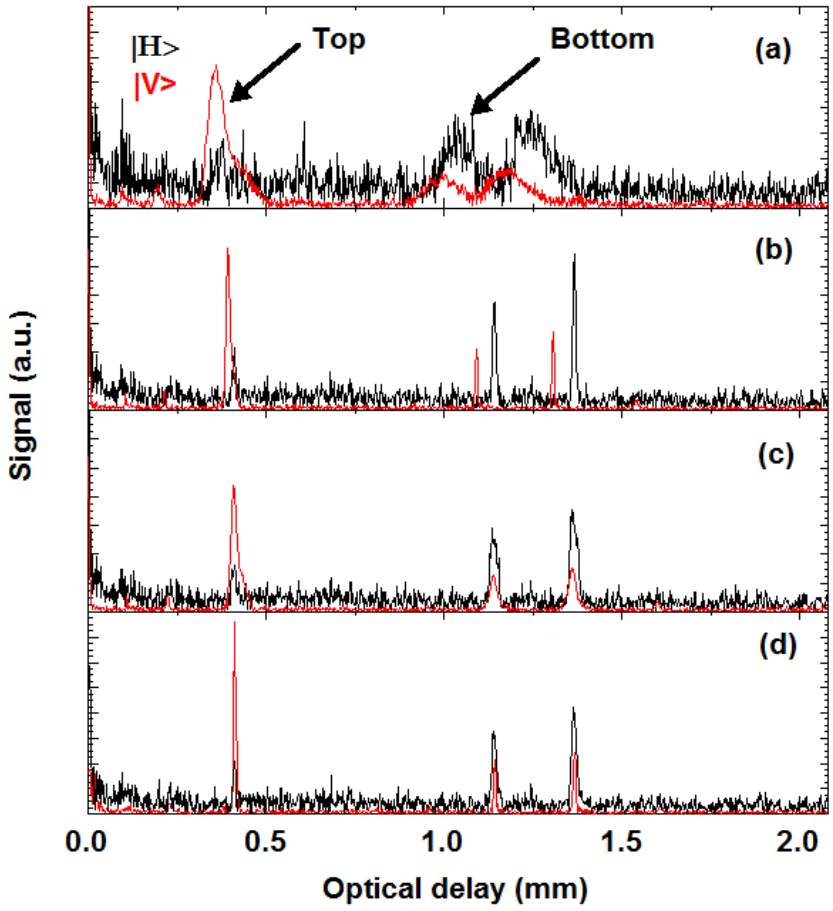

Fig. 2. Absolute value of A-lines during each step (see text).

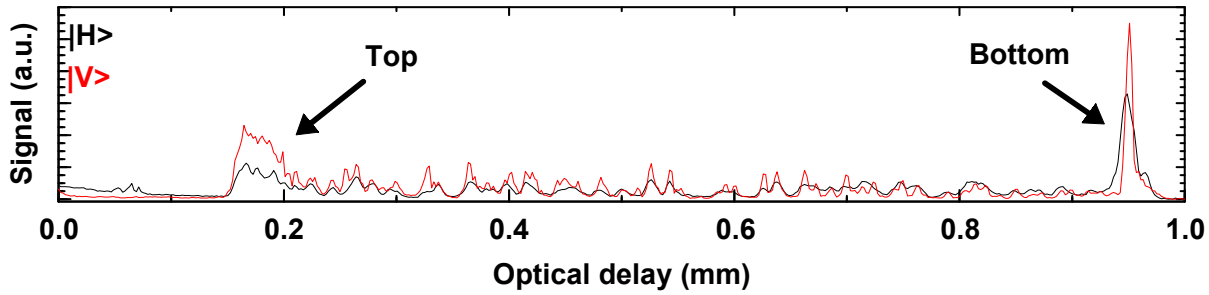

Fig. 3. OCT signals averaged over 1000 A-lines in a water droplet containing 1μm microspheres, after digital dispersion compensation.

The dispersion parameters computed from the reference images were then stored and used to digitally compensate subsequent images. The alignment between polarization states is further demonstrated with M-mode OCT of a water droplet containing point-like scatterers (Fig. 3), showing a strong correlation between peaks. Finally, we use this dispersion compensation method to perform PSOCT retardance mapping in a chicken muscle (Fig. 4), where birefringence is observed at depths up to

1mm. We note that, without the additional steps taken to align the polarized scatterers, artifacts were observed near the muscle-air interface.

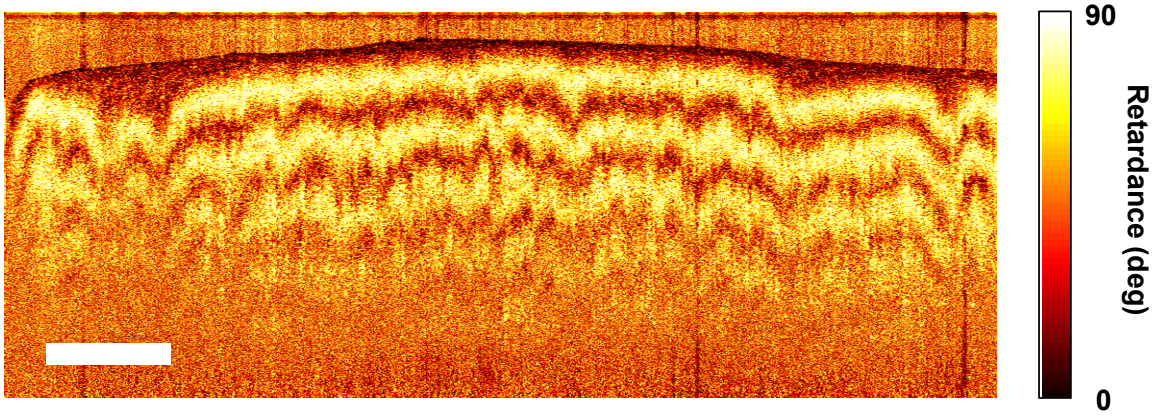

Fig. 4. B-mode retardance of chicken muscle after digital dispersion compensation (scalebar: 500μm).

4. Conclusion

In this work we have addressed the primary limitation of single-camera OCT systems that simultaneously image both polarization states. By employing a digital dispersion algorithm we can concomitantly correct for the sample dispersion, interferometer dispersion mismatch, and camera nonlinearity, relaxing the requirements on the camera alignment. We demonstrate our method using a challenging ultrahigh-bandwidth PSOCT system.

5. Acknowledgements

We acknowledge Dr. Daniel L. Marks at Duke University for technical contributions to this work. This work was supported by startup funds at the University of North Carolina at Chapel Hill.

References

[1] J. F. de Boer, T. E. Milner, M. J. C. van Gemert, J. S. Nelson, "Two-dimensional birefringence imaging in biological tissue by polarization-sensitive optical coherence tomography," *Opt. Lett*. 22:934 (1997).

[2] B. Baumann, E. Gotzinger, M. Pircher, C. K. Hitzenberger, "Single camera based spectral domain polarization sensitive optical coherence tomography," *Opt. Express* 15:1054 (2007).

[3] B. Cense, M. Mujat, T. C. Chen, B. H. Park, J. F. de Boer, "Polarization-sensitive spectral-domain optical coherence tomography using a single line scan camera," *Opt. Express* 15:2421 (2007).

[4] C. Fan, Y. Wang, R. K. Wang, "Spectral domain polarization sensitive optical coherence tomography achieved by single camera detection," *Opt. Express* 15:7950 (2007).

[5] M. Mujat, B. H. Park. B. Cense, T. C. Chen, J. F. de Boer, "Autocalibration of spectral-domain optical coherence tomography spectrometers for *in vivo* quantitative retinal nerve fiber layer birefringence determination," *J. Biomed. Opt*. 12:041205 (2007).

[6] D. L. Marks, A. L. Oldenburg, J. J. Reynolds, S. A. Boppart, "Digital algorithm for dispersion correction in optical coherence tomography for homogeneous and stratified media," *Appl. Opt*. 42:204 (2003).

[7] W. Drexler, J. G. Fujimoto, *eds*., **Optical Coherence Tomography: Technology and Applications**, J. A. Izatt and M. A. Choma, "Theory of Optical Coherence Tomography," Ch. 2, Springer, 2008.